REPORT DOCUMENTATION PAGE

Form Approved
OMB No. 0704-0188

Public reporting burden for this collection of information is estimated to average 1 hour per response, including the time for reviewing instructions, searching existing data sources, gathering and maintaining the data needed, and completing and reviewing this collection of information. Send comments regarding this burden estimate or any other aspect of this collection of information, including suggestions for reducing this burden to Department of Defense, Washington Headquarters Services, Directorate for Information Operations and Reports (0704-0188), 1215 Jefferson Davis Highway, Suite 1204, Arlington, VA 22202-4302. Respondents should be aware that notwithstanding any other provision of law, no person shall be subject to any penalty for failing to comply with a collection of information if it does not display a currently valid OMB control number. **PLEASE DO NOT RETURN YOUR FORM TO THE ABOVE ADDRESS.**

1. REPORT DATE *(DD-MM-YYYY)*
07-05-2009

2. REPORT TYPE
Journal Article

3. DATES COVERED *(From - To)*

4. TITLE AND SUBTITLE

Total and Differential Sputter Yields of Boron Nitride Measured by Quartz Crystal Microbalance (Preprint)

5a. CONTRACT NUMBER

5b. GRANT NUMBER

5c. PROGRAM ELEMENT NUMBER

6. AUTHOR(S)
B. Rubin, J. Topper, & A.P. Yalin (Colorado State University/ERC)

5d. PROJECT NUMBER

5e. TASK NUMBER

5f. WORK UNIT NUMBER
33SP0853

7. PERFORMING ORGANIZATION NAME(S) AND ADDRESS(ES)

Air Force Research Laboratory (AFMC)
AFRL/RZSS
1 Ara Road
Edwards AFB CA 93524-7013

8. PERFORMING ORGANIZATION REPORT NUMBER

AFRL-RZ-ED-JA-2009-189

9. SPONSORING / MONITORING AGENCY NAME(S) AND ADDRESS(ES)

Air Force Research Laboratory (AFMC)
AFRL/RZS
5 Pollux Drive
Edwards AFB CA 93524-7048

10. SPONSOR/MONITOR'S ACRONYM(S)

11. SPONSOR/MONITOR'S NUMBER(S)
AFRL-RZ-ED-JA-2009-189

12. DISTRIBUTION / AVAILABILITY STATEMENT

Approved for public release; distribution unlimited (PA #09241).

13. SUPPLEMENTARY NOTES
For publication in the Journal of Physics D.

14. ABSTRACT

We present differential sputter yield measurements of boron nitride due to bombardment by xenon ions. A four-grid ion optics system is used to achieve a collimated ion beam at low energy (<100 eV). A quartz crystal microbalance (QCM) is used to measure differential sputter yield profiles of condensable components from which total sputter yields can also be determined. We report total and differential sputter yields of three grades of boron nitride due to bombardment by xenon ions for ion energies in the range of 60-500 eV and ion incidence angles of 0°, 15°, 30°, and 45° from normal. Comparisons with published values are made where possible.

15. SUBJECT TERMS

16. SECURITY CLASSIFICATION OF:			17. LIMITATION OF ABSTRACT	18. NUMBER OF PAGES	19a. NAME OF RESPONSIBLE PERSON
					Dr. Justin Koo
a. REPORT	**b. ABSTRACT**	**c. THIS PAGE**	SAR	19	**19b. TELEPHONE NUMBER** *(include area code)*
Unclassified	**Unclassified**	**Unclassified**			N/A

Total and Differential Sputter Yields of Boron Nitride Measured by Quartz Crystal Microbalance (Preprint)

B Rubin, J Topper and A P Yalin
Colorado State University, Fort Collins, Colorado, 80523

We present differential sputter yield measurements of boron nitride due to bombardment by xenon ions. A four-grid ion optics system is used to achieve a collimated ion beam at low energy (<100 eV). A quartz crystal microbalance (QCM) is used to measure differential sputter yield profiles of condensable components from which total sputter yields can also be determined. We report total and differential sputter yields of three grades of boron nitride due to bombardment by xenon ions for ion energies in the range of 60-500 eV and ion incidence angles of 0°, 15°, 30°, and 45° from normal. Comparisons with published values are made where possible.

Nomenclature

A_s	=	piezoelectrically active area of QCM
E	=	beam ion energy
E^*	=	characteristic energy to describe sputtering profile
E_{th}	=	sputtering threshold energy
$J_{B,avg}$	=	time-averaged current of bombarding particles (ions and energetic neutrals)
k	=	fitting parameter
M_i	=	molar mass of species i
R	=	mass accumulation rate
Y	=	total sputter yield
α	=	polar angle of ejected sputtered particle (from target normal)
β	=	ion incidence angle relative to target normal
ϕ	=	azimuthal angle of ejected sputtered particle
ρ	=	density of target material
r_{qcm}	=	distance from target center to QCM
y_{MZ}	=	differential sputter yield found from Modified Zhang expression
y	=	differential sputter yield

I. Introduction

Ion sputtering is a primary life-limiting mechanism in electric propulsion (EP) thrusters used for satellite and space exploration [1-12]. Owing to the relatively long lifetimes (5-10+ years) of EP thruster devices and the complexity and expense of experimental tests, effects of sputter erosion and deposition are often studied with numeric codes. For erosion (lifetime) studies, the aim is to compute the amount of surface erosion due to the bombarding ions. Such modeling requires knowledge of the total sputter yields (Y) of the eroding materials at the ion conditions (energy and incidence angle) of interest. Deposition modeling additionally requires differential (angular) sputter yields ($y(\alpha,\phi)$) in order to track the trajectories of sputtered particles. Total and differential sputter yield profiles have been measured with a multitude of techniques, a partial list of which includes weight loss [10,12], collector plates [13-14], mass spectrometry [15], quartz

crystal microbalance [3-7,9-11,16-17], Rutherford backscattering [18-19], radioactive tracers [20], and cavity ring-down spectroscopy [21-22].

We are specifically interested in the sputtering of boron nitride (BN) because of its widespread use as an insulator material in the acceleration channel of stationary plasma thrusters (SPTs). Erosion of the insulator channel is the dominant thruster life-limiting mechanism in SPTs. Sputter erosion removes material from the channel wall and eventually exposes the underlying magnetic yoke, causing the magnetic field profile to be altered and the end of life to be reached. Furthermore, deposition of the sputtered BN can contaminate spacecraft surfaces (e.g. solar panels or thermal control surfaces). Despite the importance of BN erosion there is a lack of basic sputtering data on BN. Numerical modeling of thruster erosion [23-25] shows that the ions most critical to the erosion process have relatively low energy (<~100 eV). Measurements in this energy range are challenging since the low sputter yields can lead to signals below the detection sensitivity of the measurement system; additionally, it can be difficult to obtain collimated monoenergetic ion beams at these energies. The goal of the present study is to contribute towards filling this gap. In this work we detail development of an experimental configuration for low energy BN sputter measurements. We report differential and total sputter yields for several grades of BN at ion energies down to 60 eV, obtained with a QCM deposition sensor [5-7, 9-11]. In Section II we discuss the experimental apparatus and procedures used for data analysis. Section III contains a summary of the experimental results, including total and differential sputter yields of HBC, HBR, and HP grades of boron nitride under bombardment by xenon ions. Comparisons with available published values are provided. Finally, conclusions are given in Section IV.

II. Experimental Apparatus and Procedure

A. Overview of Sputter Measurement System

Total and differential sputter yields are measured using a quartz crystal microbalance (QCM) deposition monitor. The experimental apparatus is shown in figure 1. The main elements of the system have been previously described [5-7, 9-11]. In this subsection we give an overview of its essential features, while the following subsections detail specific aspects and recent modifications. An improvement relative to our past work [7] is that both weight loss and QCM measurements are performed concurrently in the same facility. The role of weight-loss measurements is discussed below. The ion source and QCM are housed within a 0.125 m^3 stainless steel vacuum chamber (43 cm ID x 76 cm long main section), equipped with a 1500 liter/s CTI-8 cryogenic pump. The chamber base pressure was 6×10^{-5} Pa giving a working pressure of approximately .8 to 1.3×10^{-2} Pa. The DC ion source with two-grid and four-grid ion optics, specially designed for low energy operation, is described below in more detail. A rotatable target-mount is positioned 23 cm downstream of the ion source. As shown in figure 1, the QCM is rotated in an arc above the target and the target itself is rotated azimuthally. Combinations of these movements allow us to probe over the hemisphere above the target, thereby obtaining differential sputter yield profiles. Both the QCM and target rotation are performed using 25000 step stepper motors, which are controlled using a motion control system (Parker CompuMotor). A personal computer with LabView is used for data logging. Detailed discussion of the QCM sensor is provided in Section IIF.

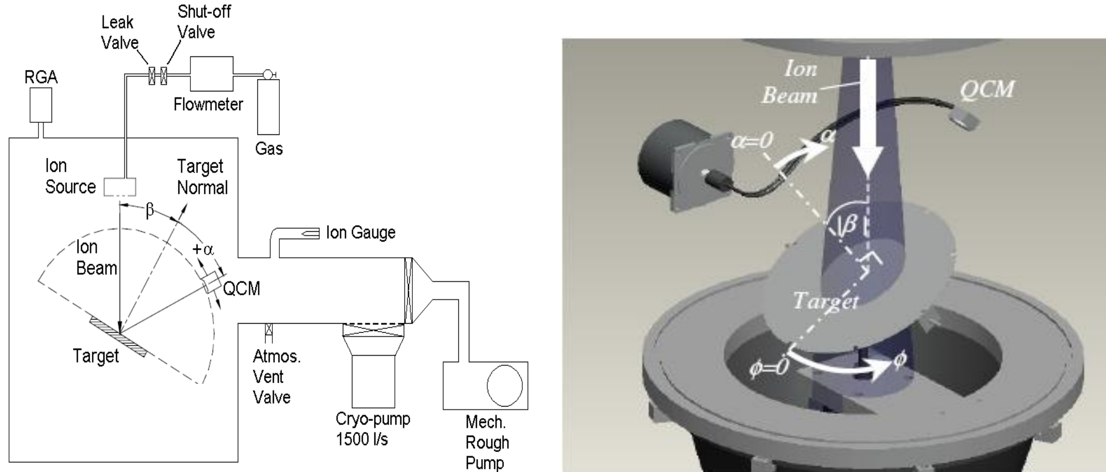

Figure 1. Left: Schematic diagram of experimental set-up. Right: Solid-model showing angle definitions.

B. Definition of Angles

The angles used to describe the direction of ion incidence and the ejections angles of sputtered particles are shown in figure 1. We define as follows: β is the incidence angle of bombarding ions measured relative to the surface normal (β=0 for normal incidence), α is the ejection polar angle of sputtered atoms measured relative to the surface normal, and ϕ is the ejection azimuthal angle of the sputtered atoms measured in the plane of the target surface (defined so that ϕ=0 is in the forward sputter direction i.e. in the forward direction of the plane containing the surface normal and the incident ion directions).

C. Ion Source

A DC Kaufman ion source using a dual thoriated tungsten filament as a discharge cathode and thoriated tungsten filament as a neutralizer is used [11]. The four-grid ion optics system, designed using an in-house ffx code [26, 27] and fabricated in-house, produces collimated beams at the low ion energies of interest to this work (20-350 eV). For higher energy measurements (350 – 500 eV), a two-grid ion optics system is used. For both grid sets, typical beam parameters include a xenon flow rate of 0.5 sccm, a beam current of 1-4 milliamps, a discharge voltage of 20 to 40 volts, and a neutralizer current of 150 % of the beam current. During measurements, the ion current leaving the source is recorded. Determination of the sputter yield requires knowledge of the current of energetic particles (ions and fast neutrals) incident on the sputtering target. As in our past work [9-11], we make corrections for charge-exchange and scattering. The charge-exchange beam generates fast neutrals which, depending on scattering angles, may bombard the target. The resulting correction is to multiply the measured source current by 0.8-0.95, depending on the chamber pressure and ion energy.

Ion source characterization was performed to determine the bombardment conditions [27]. The beam divergence angle, defined as the angle from normal including 90% of the beam current, was found as 12° from a beam profile measured with a collimated Faraday probe (the divergence angle increases slightly with beam energy) corresponding to a beam diameter of approximately 13.5 cm at the sample plane. A four-grid retarding potential analyzer (RPA) was used to measure the ion energy distribution, yielding a full width at half maximum (FWHM) of 6-19 volts, increasing with beam energy. To determine the charge state of the ions an ExB probe was used. No triply charged ions were detected. The average double-to-single number density ratio was ≤5% for beam energies between 80 eV and 250 eV, dropping with decreasing energy. For beam energies below 80 eV the number density of doubles fell below the detection limit (1%). The

doubly-charged ions have twice the energy of singles but are counted as two charges in the current measurements. Because the measured yields are relatively linear and the fraction of doubles is low, simple estimates show their effect to be negligible.

D. Boron Nitride Targets, Surface Charging and Moisture Effects

Test results reported herein are for HBC, HBR, and HP grades of Boron Nitride (BN). Each of these materials is formed by hot-pressing and corresponds to the graphite-like allotrope of BN. In the base plane, atoms are held together by strongly directed hexagonal arrays of covalent bonds, resulting in unique electrical, thermal, and mechanical properties. The HBC and HBR materials were obtained from General Electric's Advanced Ceramics (currently Momentive Performance Materials). Calcium borate is used as the binder in HBR, while no binder is used in HBC. The two grades have generally similar properties though with some differences. For example, HBR has higher thermal expansion, higher moisture absorption, and higher volume resistivity at elevated temperatures. The HP grade is obtained from Saint-Gobain and uses calcium borate as a binder. Figure 2 shows Scanning Electron Microscope (SEM) pictures of HBC grade BN in an un-sputtered state and after 15 hours of sputtering by a 250 eV Xe ion beam. Little change can be detected in the surface structure, and none which can be positively attributed to the effects of sputtering.

Our past measurements of insulator materials including boron nitride have shown effects of surface charging and the importance of appropriate neutralization [9-11]. Similar surface charging effects have been observed by Zhang et al. [28] and Nikiporetz et al. [29]. In order to neutralize the surface charge, a plasma bridge neutralizer (PBN) is placed in the chamber close to the target. Details on the neutralization scheme are discussed in our past work [9-11]. Operating conditions of the PBN are an emission current of 10-15 mA and a Xe mass flow rate of 0.5 sccm. The PBN was biased at negative 15 V relative to ground potential.

The total sputter yields are also measured using a standard weight loss technique, but the results displayed poor reproducibility and are not reported here. One of the factors affecting the accuracy of the weight loss measurement is moisture absorption by the samples. Effects of moisture absorption and associated mass change are observed for all grades of BN, although different grades of BN exhibit different amount of moisture pick-up [10,11]. HBC has the lowest moisture pickup, followed by HBR and HP. The latter two can maintain appreciable amounts of moisture even after storage in a dry environment. This behavior is most probably related to the fact that in both HBR and HP grades contain a calcium borate binder. These effects are expected based on moisture absorption information provided in the material datasheets. Similar effects were reported by Garnier [30].

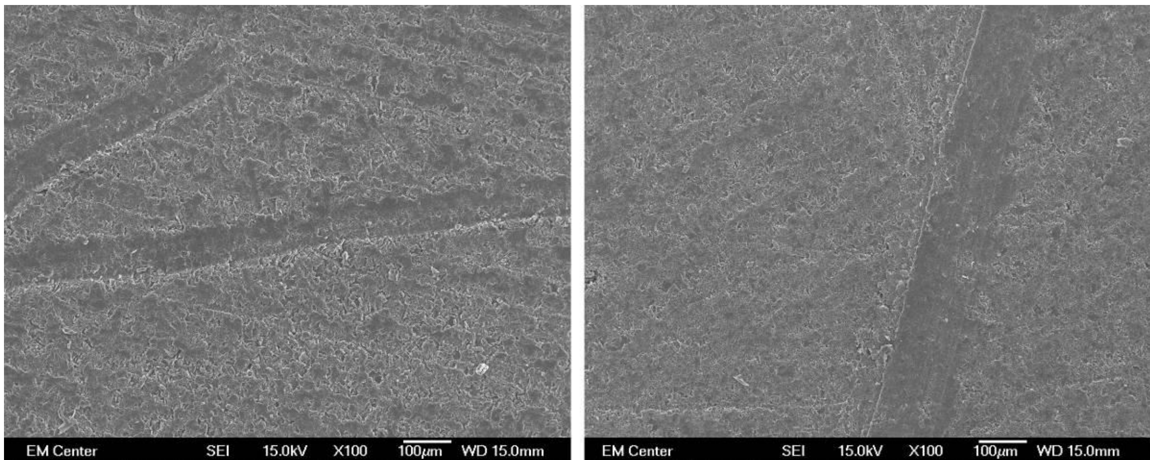

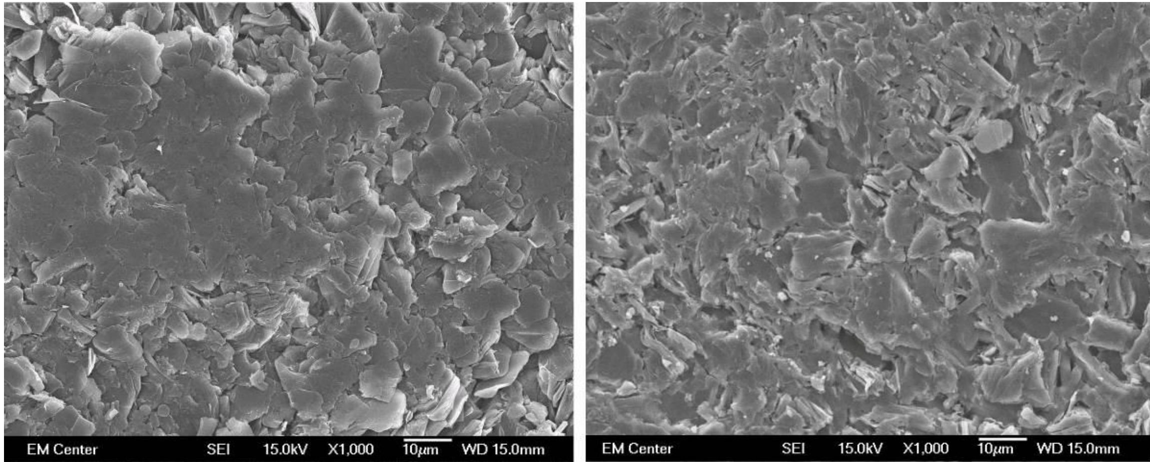

Figure 2. Scanning Electron Microscope images of HBC BN surface. Left: Unsputtered surface. Right: Sputtered with 250 eV Xe+ ions for 15 hours.

For HBR the mass buildup (for the resolution of our measurements) levels off after approximately one hour after venting the chamber and exposing the targets to the atmosphere. In comparison to HBR BN, we find the HP mass to increase at a higher rate and for a longer duration (more than 24 hours). As means of illustration, figure 3 shows mass buildup on HP BN samples after removal from the vacuum chamber (sample mass is approximately 150 g). Zero mass in figure 3 corresponds to the sample mass after 90 minutes of atmospheric exposure, and zero time to 90 minutes after the sample was removed from the vacuum chamber. Mass build-up in the first 90 minutes is at an even higher rate. In summary, the large mass buildup (and variation of individual samples) relative to the total mass change of a typical sputter test (~2-10 mg) precludes accurate sputter yield determination from mass loss measurements in our current setup. Of course, such effects do not influence QCM measurements.

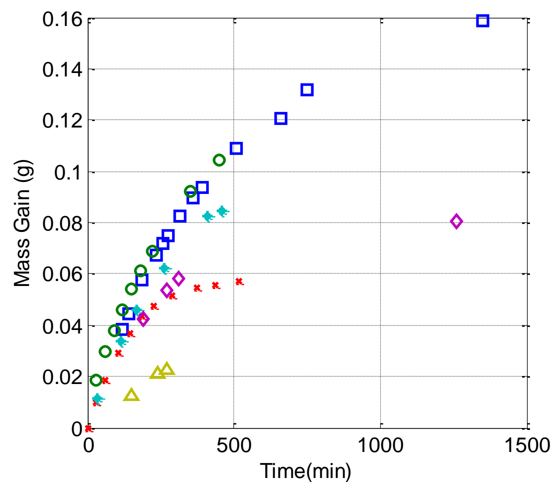

Figure 3. Mass change as a function of time for six different HP BN samples. Zero time corresponds to 90 minutes after removal from vacuum chamber, and zero mass is the sample mass at the corresponding time.

Another factor that can influence weight loss measurements is xenon ion implantation into the sample. If a significant number of xenon ions are implanted in the sample, the measured mass

loss and apparent sputter yield would be reduced. To check the influence of ion implantation, X-ray photoelectron spectrometry (XPS) analysis was performed on a HBC BN sample using a PHI 5800 XPS system. An un-used sample was sputtered for 15 hours with a 250 eV ion beam after which XPS analysis was performed. The analysis has detected implanted xenon with an atomic fraction of 0.1%. Angularly resolved XPS measurements showed that xenon is implanted only in a thin near-surface layer. The measured atomic fraction versus angle is shown in figure 4. As expected, the atomic fraction increases with the angle, confirming that the depth of the xenon implantation does not exceed few nanometers. From the point of view of weight loss, simple numeric estimates show that the mass of implanted xenon is negligible compared to the mass change due to sputtering.

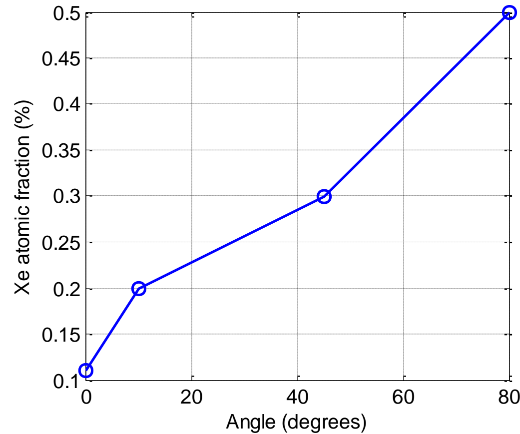

Figure 4 . Angularly resolved XPS measurements of Xe in BN target.

E. Boron Nitride Sputter Products

In deposition mode, the QCM allows determination of differential sputter yields through measurement of mass accumulation (of sputtered particles) on its surface. For condensable components, sticking coefficients are assumed to be unity. Note that sticking coefficients for “new layers” and very thin layers (typically 10’s of Angstroms) may be less than unity, but once a sufficient layer thickness of a given material has accumulated, sticking coefficients for condensables are generally unity [31]. For BN, the sputtered particles may consist of a mix of condensable and non-condensable components.

To study the chemical composition of the layer deposited on the QCM surface during the BN sputter yield measurements, the surface of the QCM was analyzed using XPS. Both boron and nitrogen 1s spectral lines were detected from the QCM surface layer with the boron fraction being approximately five and a half times that of nitrogen. The B1s spectral line shapes obtained from the XPS analysis of the QCM surface are presented in figure 5. According to the NIST XPS database [32], the B1s line of graphitic BN is at 190.5 eV. There is some variation in reported line locations of B1 [32], but the consensus is that pure atomic boron is at 186-188 eV, boron from BN is at ~190-191 eV, and B from B_2O_3 is at ~192-194 eV. The salient point is that for the QCM, boron is detected as B_2O_3 and not as BN, while for the BN surface, B is detected as both BN and B_2O_3. The presence of the B_2O_3 oxide in both cases is due to atmospheric exposure. This observation, taken with the lack of BN from the QCM surface, indicates that the BN target sputters predominantly as B and N atoms, of which the B atoms condense (deposit) on the QCM surface.

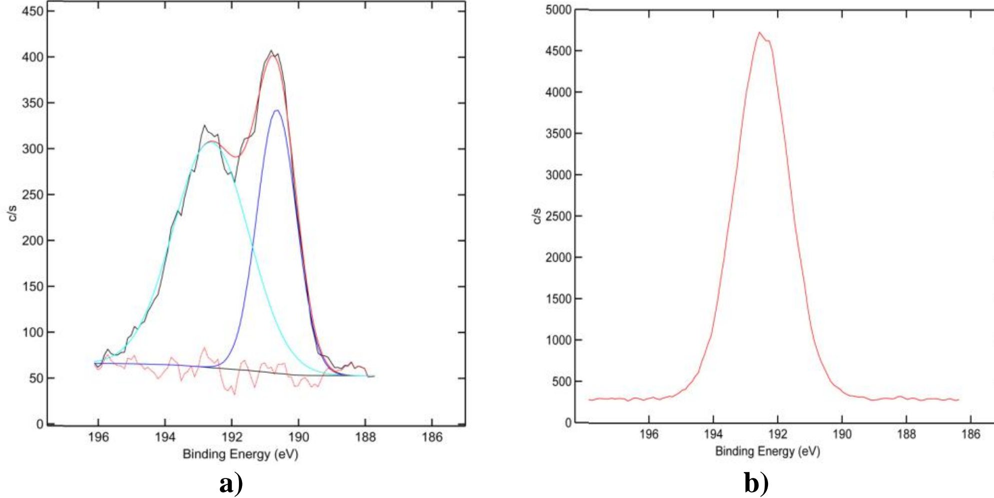

Figure 5. XPS results for the HBC BN target (left) and QCM surface (right). For the HBC BN target, fitted peaks (and their sum) are shown. See text.

Sputtering as atoms is also consistent with past mass spectrometry results [1,33] and multi-component sputtering theory. The XPS analysis of a sputtered BN sample performed by Garnier [30] demonstrated little variation between the boron and nitrogen fractions in the sample before and after sputtering, which suggests that boron and nitrogen are sputtered at approximately equal rates as would be expected based on the bulk composition. Therefore, we expect the full BN yield to be related to the deposited condensable yield through (1):

$$Y_{total} = Y_{QCM} \cdot \frac{M_B + M_N}{M_B} \quad (1)$$

where M_B is the mass of boron, M_N is the mass of nitrogen, Y_{QCM} is the QCM-measured yield, and Y_{total} is the expected total yield, based on the above assumptions (this equation applies for both differential and total yields).

F. QCM Sensor and Measurement Proceedure

We use a Sigma Instruments SQC-339 Deposition Controller that reads the crystal frequency to 0.001 Hz and an RC-cut quartz crystal as opposed to the more conventional AC-cut crystal. The RC-cut crystal, manufactured by Tangidyne Corporation, is very accurate for deposition of thin films. Increased sensitivity is achieved by adjusting the stress coefficients of the quartz plate using advanced fabrication methods

The quartz crystal resonance frequency is extremely sensitive to temperature variation, so the QCM should be maintained at constant temperature during measurements. A PolyScience 9002 Programmable Digital Temperature Controller with refrigerating/heating circulator is used to control the temperature of the QCM. The water circulates through the stainless steel body of the QCM housing, and the temperature of the water in the bath is controlled to ±0.01°C. As the crystal is moved to different positions during the measurement, the heat flux to it varies due to the change in relative position of the QCM and the heat sources in the system (ion source and PBN). Therefore, although the temperature of the water stays constant, the actual crystal temperature is different at different locations (α angles). A K-type thermocouple wire embedded in a copper holder silver-soldered to the back of the QCM crystal holder is used to monitor QCM temperature. When the QCM is moved to a new measurement position, the QCM temperature is monitored, and sputter yield measurements are started only after the temperature of the crystal has stabilized.

For a given incidence angle β (obtained by tilting the target), the differential sputtering profile is obtained by measuring the sputter yield over two chords above the target: ϕ=0° /180° and ϕ = 60°/240° (where the latter, by symmetry, also corresponds to ϕ=120°/300° for azimuthally symmetric sputtering profiles). A total of 34-36 positions above the target are typically sampled. At a given measurement point the volumetric differential sputter yield, $y(\alpha,\phi)$, in units of mm^3/C/sr, is determined using:

$$y(\alpha,\phi) = \left[R(\alpha,\phi) r_{qcm}{}^2\right] \Big/ \left[\rho J_{B,avg} A_s\right] \quad (2)$$

In (2), $R(\alpha, \phi)$ is the measured mass accumulation rate (found from the QCM's deposition monitor device), ρ is the density of the target material, $J_{B,avg}$ (C/s) is the time-averaged current of bombarding particles (ions and energetic neutrals) incident on the target, r_{qcm} is the distance from the target center to the QCM (17.4 cm), and A_s is the QCM sensor area (0.535 cm^2). The quantity $A_s/r_{qcm}{}^2$ corresponds to the solid angle that the QCM sensor subtends while $R(\alpha, \phi)/\rho J_{B,avg}$ corresponds to the volume of sputtered material per bombarding charge. It is important to emphasize that the directly measured quantity is the mass buildup of condensable particles on the QCM and the volumetric differential sputter yield should be considered in this way. (In fact the "volume" may not really correspond to any physically observed volume since it corresponds to the equivalent volume due to the mass of the *deposited condensable material* if one uses the density of the full *target material*; of course conversion to the deposited mass yield simply requires removing the density from (2)). Finally, as discussed above, equation (1) can be used to convert the measured condensable yield (from (2)) to the corresponding full BN yield.

G. QCM Signal Analysis.

Analysis and fitting of differential sputter yield profiles requires appropriate functional forms. At our conditions, stopping is predominantly due to elastic (nuclear) collisions and is generally in the linear cascade regime (emitted particles are secondary or higher generation recoils) or single knock-on regime (emitted particles are primary recoils) [1]. A classical theory for the linear cascade regime was originally developed by Sigmund [35]. Independent of ion incidence angle, the original Sigmund theory predicts sputtering profiles that are azimuthally symmetric and approximately diffuse in shape, corresponding to cosine-like profiles of the form $y\text{\textasciitilde}\cos(\alpha)^n$ (n=1 for a diffuse profile). More recent experimental and numerical studies show a range of profile shapes. For normally incident ions on polycrystalline and amorphous targets, cosine-like profiles are generally observed with increasingly under-cosine shapes as ion energy is lowered and increasingly over-cosine shapes for higher ion energies [5-7,9-10,15,35-37]. For obliquely incident ions at relatively high ion energy, observed profiles also tend to be azimuthally symmetric. However, for lower ion energies the measured profiles tend to be asymmetric with increased sputtering in the forward direction [5-7,9-10,16,20,35]. Similar profiles have been modeled on a theoretical basis [37-39].

As a means to describe the measured differential sputter yield profiles we use expressions from Zhang [40], based on work from Yamamura [38-39], to which we introduce two fit parameters. We term the resulting expressions as Modified Zhang (MZ) [7].

$$y_{MZ} = \frac{Y}{1-\sqrt{\frac{E^*}{E}}\cos(\beta)} \cdot \frac{\cos(\alpha)}{\pi}\left[1-\frac{1}{4}\sqrt{\frac{E^*}{E}}\left(\cos(\beta)\gamma(\alpha)+\frac{3}{2}\pi\sin(\beta)\sin(\alpha)\cos(\phi)\right)\right] \quad (3a)$$

$$\gamma(\alpha)=\frac{3\sin(\alpha)^2-1}{\sin(\alpha)^2}+\frac{\cos(\alpha)^2\left(3\sin(\alpha)^2+1\right)}{2\sin(\alpha)^3}\ln\left(\frac{1+\sin(\alpha)}{1-\sin(\alpha)}\right) \tag{3b}$$

where y_{MZ} is the differential sputter yield, Y is the total sputter yield, E is the ion energy, E^* is a characteristic energy describing the profile shape, and the angles are as defined above (the expression is properly normalized so that integrating the differential sputter yield, y_{MZ}, over the sputtering hemisphere gives Y). The approach decouples the amplitude of the angular profiles from their shape through the use of Y and E^* respectively. More recent work by Zhang et al [40] also discusses the use of a varying energy parameter. In general, rather than using the MZ expressions for *a priori* calculation, we treat Y and E^* as free fit-parameters which we determine from (least-squares fitting) experimental data. Note that profile shapes are determined by the ratio E^*/E and for high ion energy ($E^*/E << 1$) the MZ expression reduces to the diffuse yield ($y=Y\cos(\alpha)/\pi$).

H. Measurement Procedure

Targets are deliberately pre-sputtered to better represent the conditions found in long-duration EP operating applications. Pre-sputtering of HBC and HBR samples was by a 500 eV ion beam with a current density of ~0.1 mA/cm² for 15 hours the HP sample was pre-sputtered by a 750 eV ion beam with a current density of ~1 mA/cm² for 2 hours. An order-of-magnitude estimate for the typical dose of incident ions on a target prior to testing is 10^{19} ions/cm^2 (corresponding to thickness of several microns). Target contamination effects are estimated to be negligible, since for typical conditions the flux of ions incident on the target is approximately 10 times higher than the flux of nitrogen (the major contaminant) to the target [7]. The samples were heated under the chamber filaments for at least 30 minutes prior to sputtering to remove the moisture and to reach a thermal steady-state condition. Test durations are fixed such that the QCM has time (at each position) to sufficiently stabilize relative to thermal and background noise. Test times vary from several hours for higher energy tests to as long as 20 hours for lower energy tests.

III. Measurement System Validation

Validation of our total sputter yield measurements is performed by using molybdenum as a control. While there is variation in data from different research groups, molybdenum sputter yields are reasonably well characterized [3,6,7]. We have measured the total sputter yield of Mo at normal incidence at energies of 150, 250 and 350 eV. As shown in figure 6, the total yields found from the Y parameter of the best-fit MZ profile are self-consistent and in reasonable agreement with the Yamamura and Tawara curve fit [42-43]. The yields are somewhat lower than those previously measured using the same apparatus with two-grid ion optics (shown as CSU 2007) though the difference is within experimental uncertainty [7]. Although our values are approximately a factor of two lower then Kolasinski's (measured by etching a thin Mo layer off the QCM surface), they are in good agreement with the data of Doerner [44] (weight loss method). These results are taken as validation of the measurement methods and in particular of the assumption that the sticking coefficient of the QCM may be taken as unity for condensables.

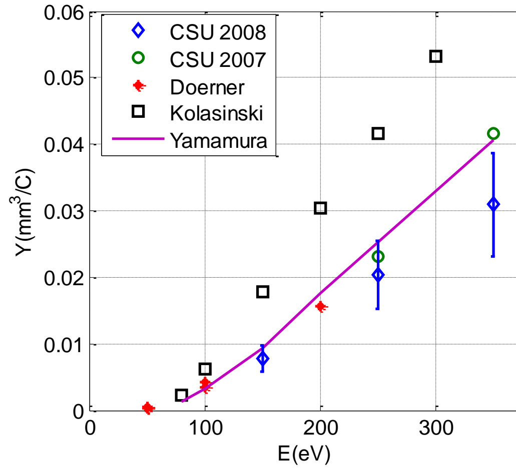

Figure 6. Total sputter yield from QCM versus ion energy for normal incidence, Xe^+ on Mo.

IV. Results & Discussion

A. Total Sputter Yields

Figure 7 shows total sputter yields of the three BN grades, determined from the *Y* parameter of the best-fit MZ profile (equivalent to integrating the best-fit profile) as a function of ion energy for normal incidence. The total yields of figure 7 (and figure 8) are only due to condensables. The measurements of total sputter yield values are performed multiple times for the majority of the data points. Measurements in the energy range of 60-350 eV are preformed using the four-grid ion optics, while the range of 350-500 eV uses the two-grid ion optics. For the cases when several measurements were done at the same conditions, the average value is reported. Experimental uncertainty and error bars on measured differential sputter yields are estimated from the repeatability of the sputter yield measurements.

An equation developed by Bohdansky [45] is used to fit HBC BN data:

$$Y = k\left[1-\left(\frac{E_{th}}{E}\right)^{2/3}\right]\left[1-\frac{E_{th}}{E}\right]^2 \tag{4}$$

Bohdansky altered the original Sigmund expression [34] to better match low energy sputter yields The values of k and E_{th} from a least squares fit of HBC data are 0.053 and 32 eV, respectively. The resulting fit is presented in figure 7. An expression from Zhang [40] for the energy dependence of the total sputter yield is also fitted to the experimental data, but the fit does not represent the experimental data as well as that from Bohdansky, especially at low energies. The threshold energy obtained from the Zhang fit was 57 eV.

The variation of total sputter yield with incidence angle at a fixed energy of 100 eV is shown in figure 8. A semi-empirical equation from Yamamura [43] is fitted to the HBC data and is also shown. The trend in both experimental data and Yamamura fit is for the yields to somewhat increase over the range of angles measured, consistent with past research [43].

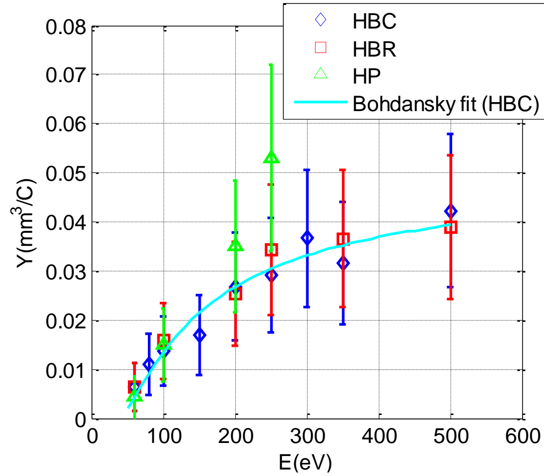

Figure 7. Total condensable sputter yield from QCM versus ion energy for normal incidence.

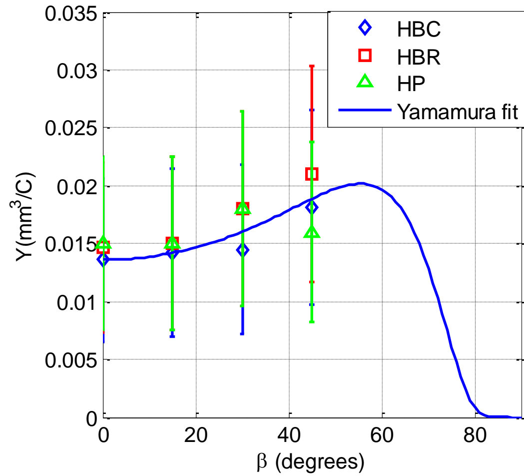

Figure 8. Total condensable sputter yield from QCM versus incidence angle for 100 eV ion energy.

Where possible, we compare our total sputter yields with measurements and modeled values from other research groups. Figure 9 shows our recent measurements for HBC BN along with weight loss measurements by Semenov [46], Garnier [30], Abashkin [47], Kim [48], and modeled values from Yim [23]. In this case we have scaled our yields using (1) to represent full BN sputtering yields (not just the measured condensables). Not all of the authors specify the grade of BN used. The values we are currently reporting are high relative to past measurements. Exact reasons for the discrepency are unknown but possibilities are as follows. The difference in the measured sputter yields can be attributed to the difference in the properties of different BN grades. Comparison against weight loss measurements may be influenced by moisture effects. Also, if samples have been heated, it is possible that surface changes have been induced. Finally, inadequate surface neutralization may lead to low apparent yields. The validation measurements presented in section IIH suggest that if a systematic error is present in our data, it results in lower, not higher, sputter yield values. The values reported here are also higher then the values we have previously reported in Ref. 10, obtained using the weight loss method in different vacuum chamber. The most plausible reasons are inadequate surface charge neutralization or variations in current density values used in the previous work.

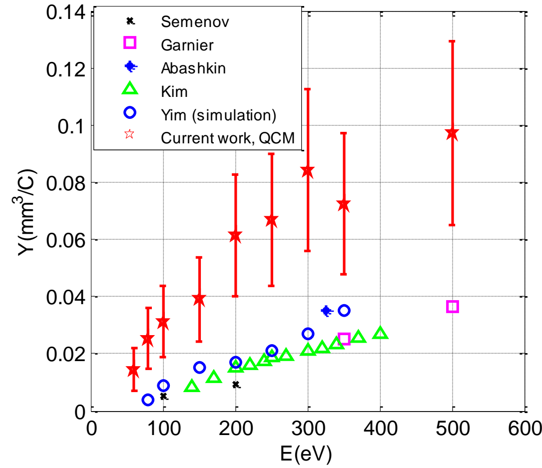

Figure 9. Total BN sputter yields as compared with published values.

B. Differential Sputter Yields

As described in Section IIE, MZ expressions are used to fit the profiles and the parameter *E*/E* describes the *shape* of the profile. Figure 10 shows the variation in *E*/E* for normal incidence as a function of ion energy for the three grades of BN. The parameter *E*/E* tends to increase with energy for all grades of BN. Figure 11 shows the variation in *E*/E* at 100 eV as a function of incidence angle for the three grades of BN. For HBC and HP grades the value of the parameter is almost independent of the incidence angle, for HBR it increases with the incidence angle. Error bars are estimated from the repeatability of the differential sputter yield measurements.

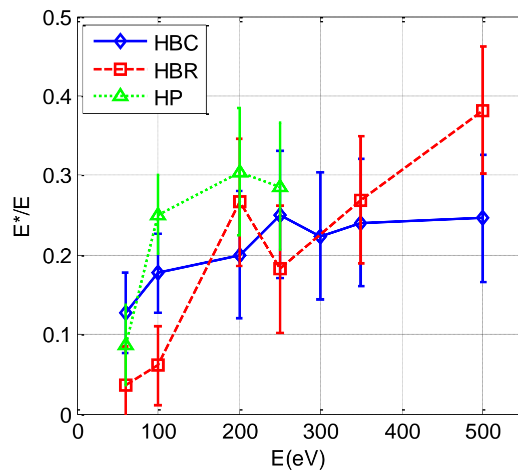

Figure 10. *E*/E* versus ion energy for normal incidence. Points are joined with straight lines to guide the reader.

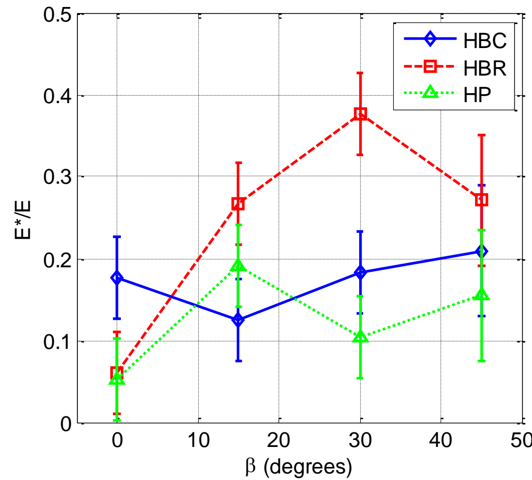

Figure 11. *E*/E* versus incidence angle for 100 eV ion energy.

Examples of comparison between measured (raw) QCM data and fitted MZ profiles are given in figure 12 Both plots are for xenon ion energies of 250 eV on HBC BN. The left plot is for normal incidence and the right plot for 30° incidence. The plots include QCM measured points, best-fit MZ profiles, and (for comparison) diffuse profiles with the same total yield. One can see relatively good agreement between the measured profiles and MZ profiles. The fitted normally incident profile is azimuthally symmetric. The profile for 30° incidence is measured in the forward/backward plane (ϕ=0/180°) and shows a forward sputter lobe (negative alpha) and reduced sputtering in the backward direction (positive alpha). In general, the MZ expressions provide reasonable descriptions of the measured profiles. The asymmetry of the non-normal incidence profiles and the disagreement with diffuse profiles in all cases illustrates the inadequacy of simply assuming diffuse profile shapes as has been done in some past research.

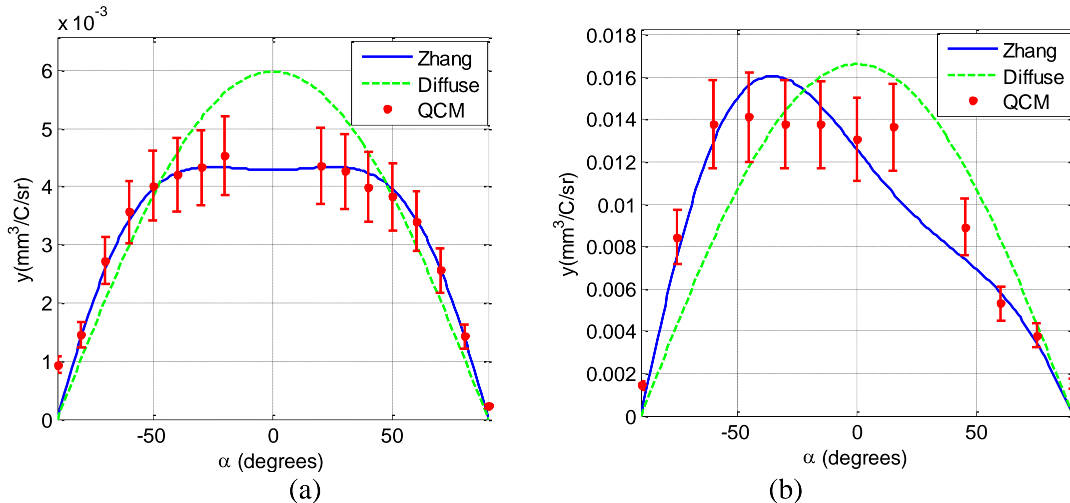

Figure 12. Example of QCM data with best-fit MZ profiles 250 eV ions on HBC at normal incidence, (a) and for 250 eV ions on HBC BN at 30° (b).

In figures 13-14, examples of the best-fit MZ differential sputter yields are shown using colored hemispheres. Colors (indicated in legend) correspond to the yield in the given direction. For normal incidence the profile is azimuthally symmetric, while for increasingly non-normal incidence the profiles show increasing forward sputter lobes. For 15° incidence the profile is already significantly azimuthally asymmetric.

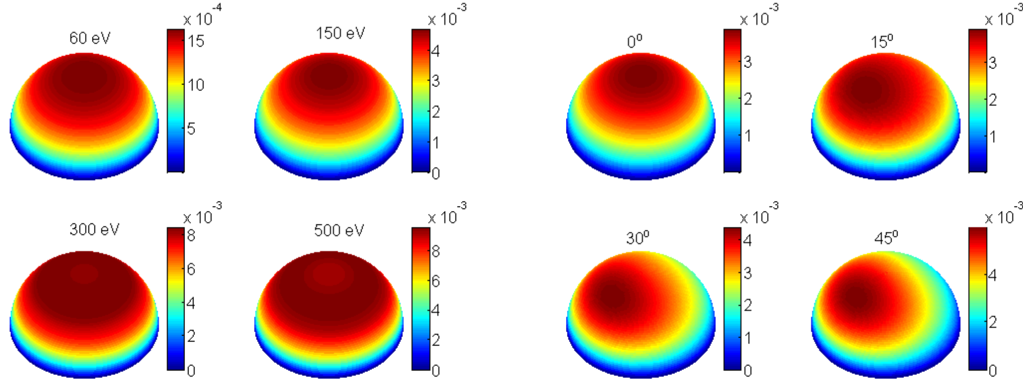

Figure 13. Differential sputter yield profiles for HBC grade BN. Left: Normal incidence and different beam energies. Right: Varying incidence angles at a beam energy of 100 eV.

In Tables 1-3 the best-fit MZ values are presented for all conditions and grades studied. The trends are generally similar to the ones presented above. Also, at non-normal incidence HBR has higher sputter yields than HBC and HP (for the latter non-normal measurement was performed only at 100 eV). Two total yield values are given for each condition: the directly measured condensable yield Y_{cond}, and the scaled value from (1), representing full BN sputtering, Y_{BN}.

Table 1. Total Sputter Yields (Y) and Characteristic Energies ($E*$) of HBC BN.

Ion Energy (eV)	Incidence Angle	Y_{Cond} (mm^3/C)	Y_{BN} (mm^3/C)	$E*$ (eV)
60	0	0.0063	0.0145	8
100	0	0.0136	0.0312	18
100	15	0.0142	0.0327	13
100	30	0.0145	0.0333	18
100	45	0.0181	0.0417	21
150	0	0.0170	0.0390	13
200	0	0.0268	0.0614	40
250	0	0.0291	0.0669	63
250	15	0.0234	0.0539	65
250	30	0.0287	0.0660	96
250	45	0.0258	0.0594	86
300	0	0.0367	0.0842	67
350	0	0.0316	0.0726	84
350	15	0.0200	0.0459	97
350	30	0.0243	0.0559	148
350	45	0.0308	0.0707	163
500	0	0.0423	0.0973	123
500	15	0.0473	0.109	150
500	30	0.0485	0.112	207
500	45	0.0545	0.125	231

Table 2. Total Sputter Yields (*Y*) and Characteristic Energies (*E**) of HBR BN.

Ion Energy (eV)	Incidence Angle	Y_{Cond} (mm^3/C)	Y_{BN} (mm^3/C)	*E** (eV)
60	0	0.064	0.015	2
100	0	0.0158	0.036	6
100	15	0.0185	0.0425	27
100	30	0.0218	0.0502	38
100	45	0.0233	0.0535	27
200	0	0.025	0.058	53
250	0	0.034	0.079	46
250	15	0.0276	0.0634	58
250	30	0.0566	0.130	69
250	45	0.0497	0.114	97
350	0	0.0365	0.0838	94
350	15	0.0328	0.0753	134
350	30	0.0514	0.118	135
350	45	0.0644	0.148	182
500	0	0.0388	0.089	191
500	15	0.0669	0.154	213
500	30	0.0657	0.151	250
500	45	0.101	0.233	261

Table 3. Total Sputter Yields (*Y*) and Characteristic Energies (*E**) of HP BN.

Ion Energy (eV)	Incidence Angle	Y_{Cond} (mm^3/C)	Y_{BN} (mm^3/C)	*E** (eV)
60	0	0.004	0.010	5
100	0	0.015	0.034	25
100	15	0.015	0.034	19
100	30	0.018	0.041	10
100	45	0.016	0.037	15
200	0	0.035	0.080	61
250	0	0.053	0.122	71

V. Conclusions

We report total and differential sputter yield measurements for three grades of BN: HBC, HBR, and HP in the energy range of 60-500 eV. Measurements have been performed using a QCM measurement approach for differential sputter yield profiles and total sputter yield of

condensable components. Total yields are found from the integrated profiles. Using a novel four-grid source we have performed the first, to our knowledge, measurements of BN sputtering below 100 eV.

The numerical models, previously published experimental data and our study of the QCM surface layer composition indicate that sputtering is predominantly as atoms (with boron atoms captured by the QCM, but not nitrogen atoms). This information is critical for interpretation of our QCM measurements and is also important for interpretation of future laser diagnostics systems based on CRDS which will measure only boron contributions[22]. We observe higher yields relative to published data. Possible reasons for this are discussed and are under ongoing investigation. In comparison to a representative refractory metal such as molybdenum, we find comparable volumetric yields for BN, though the corresponding BN mass- (or atomic-) based yields are still ~5x lower due to the lower density of BN.

We find that the fitted MZ profiles provide a reasonable description of the measured yields. The shapes (E^*/E values) for the three grades of BN are all relatively similar and show azimuthally symmetric behavior at normal incidence and forward/backward sputtering features at oblique incidence There is a critical need in the EP community for low ion energy sputter measurements of BN, and the present contribution is a step forward filling this gap. The results presented here are part of a comprehensive study currently underway. Upcoming and ongoing work aims to measure the BN sputtering over a broader range of sputtering conditions and includes study of variation of BN sputter yields with temperature.

Acknowledgments

The authors would like to thank Air Force Research Labs (Edwards Air Force Base, CA) for funding support. The authors also thank Paul Wilbur (Colorado State University) for initial development of the QCM apparatus, John Williams (Colorado State University) for assistance with the QCM apparatus and ion source, Casey Farnell (Colorado State University) for additional assistance with the ion beam profiling equipment, and Cody Farnell (Colorado State University) for designing the four-grid ion optics.

References

[1] Betz G and Wien K 1994 Energy and angular distributions of sputtered particles International *J.Mass Spectrometry and Ion Processes* **140** 1-110

[2] Tartz M, Neumann H, Fritsche B, Leiter H and Esch J 2004 Investigation of sputter behaviour of ion thruster grid materials *40th Joint Propulsion Conf. (Ft. Lauderdale, FL)* AIAA Paper 2004-4114

[3] Kolasinski R D 2005 Oblique angle sputtering yield measurements for ion thruster grid materials *41st Joint Propulsion Conf. (Tucson AZ)* AIAA paper 2005-3526

[4] Kolasinksi R D, Polk J E, Goebel D and Johnson L J 2006 Carbon sputtering yield measurements at grazing incidence *42nd Joint Propulsion Conf. (Sacramento, CA)* AIAA 2006-4337

[5] Zoerb K A, Williams J D, Williams D D and Yalin A P 2005 Differential sputtering yields of refractory metals by xenon, krypton, and argon ion bombardment at normal and oblique incidences *29th Int. Electric Propulsion Conf. (Princeton, NJ)* IEPC-2005-293

[6] Yalin A P, Williams J D, Surla V, Wolf J and Zoerb K A 2006 Azimuthal differential sputter yields of molybdenum by low energy ion bombardment *42nd Joint Propulsion Conf. (Sacramento, CA)*AIAA paper 2006-4335

[7] Yalin A P, Williams J D, Surla V and Zoerb K A 2007 Differential Sputter Yield Profiles of Molybdenum due to Bombardment by Low Energy Xenon Ions at Normal and Oblique Incidence *J.Phys.D. Appl. Phys.* **40** 3194-3202

[8] Polk J E 1999 An overview of the results from an 8200 hour wear test of the NSTAR ion thruster paper *35th Joint Propulsion Conf.* AIAA paper 99-2446
[9] Yalin A, Rubin B, Domingue S, Glueckert Z and Williams J 2007 Differential Sputter Yields of Boron Nitride, Quartz, and Kapton Due to Low Energy Xe^+ Bombardment *43rd Joint Propulsion Conf. (Cincinnati, OH)*AIAA paper 2007-5314
[10] Rubin B, Topper J and Yalin A 2007 Total and Differential Sputter Yields of Boron Nitride Measured by Quartz Crystal Microbalance and Weight Loss *30th Int. Electric Propulsion Conf. (Florence, Italy)* IEPC-2007-074
[11] Topper J L, Rubin B, Farnell C C, and Yalin A P 2008 Preliminary Results of Low Energy Sputter Yields of Boron Nitride due to Xenon Ion Bombardment, *44th Joint Propulsion Conf. (Hartford, CT)* AIAA paper 2008-5092.
[12] Yalin A P, Surla V, Farnell C, Butweiller M, and Williams J D 2006 Sputtering Studies of Multi-Component Materials by Weight Loss and Cavity Ring-Down Spectroscopy, *42nd AIAA Joint Propulsion Conf. (Sacramento, CA)*AIAA paper 2006-4338
[13] Chiplonkar V T and Rane S R 1965 Dependence of angular distribution of sputtering by positive ions from metal targets on the impact angle *Indian J. Pure Appl. Phys.* **3** 161
[14] Tsuge H and Esho S 1981 Angular distribution of sputtered atoms from polycrystalline metal targets *J. Appl. Phys.* **52** 4391-95
[15] Wucher A and Reuter W 1988 Angular distribution of sputtered particles from metals and alloys *J. Vac. Sci. Tech. A* **6** 2316-18
[16] Mannami M, Kimura K and Kyoshima A 1981 Angular distribution measurements of sputtered Au atoms with quartz oscillator microbalances *Nucl. Instrum. Meth.* **185** 533-37
[17] Wickersham C E and Zhang Z 2005 Measurement of angular emission trajectories for magetron-sputtered tantalum *J. Electron. Mater.* **34** 1474-79
[18] Shutthanandan V, Ray P, Shivaparan N, Smith R, Thevuthasan T and Mantenieks M 1997 On the measurement of low-energy sputtering yield using rutherford backscattering spectrometry *25th Int. Electric Propulsion Conf. (Cleveland, OH)* IEPC-97-069
[19] Mantenieks M, Foster J, Ray P, Shutthanandan S and Thevuthasan T 2001 Low energy xenon ion sputtering yield measurements *27th Int. Electric Propulsion Conf. (Pasadena, CA)* IEPC-01-309
[20] Kundu S, Ghose D, Basu D and Karmohapatro S B 1985 The angular distribution of sputtered silver atoms Nuclear Instruments and Methods in Physics Research B **12** 352-57
[21] Surla V and Yalin A P 2007 Differential sputter yield measurements using cavity ring-down *Appl. Optics* **46** 4057-64
[22] Yalin A, Tao L, Yamamoto N, Smith T and Gallimore A 2007 Boron Nitride Sputter Erosion Measurements by Cavity Ring-Down Spectroscopy *30th Int.l Electric Propulsion Conf. (Florence, Italy)* IEPC-2007-075
[23] Yim J 2008Computational Modeling of Hall Thruster Channel Wall Erosion Ph.D. Dissertation, University of Michigan
[24] Cheng S 2002Computational Modeling of a Hall Thruster Plasma Plume in a Vacuum Tank MS Thesis Massachusetts Institute of Technology
[25] Ustarroz J, Caro I, Corengia P, Garmendia I, Marcos J, Ahedo E and Gonzales del Amo J 2007 Specific laboratory testing equipment & methodology for sputtering tests of electric propulsion materials *30th Int. Electric Propulsion Conf. (Florence, Italy)* IEPC-2007-167.
[26] Farnell C 2007 Performance and Lifetime Simulation of Ion Thruster Optics Ph.D. Dissertation, Colorado State University
[27] Rubin B, Topper J and Yalin A (preprint) QCM based system for high-sensitivity differential sputter yield measurements to be submitted to *Rev.Sci.Instr*.
[28] Zhang L and Zhang LZ 2005 Anisotropic energy distribution of sputtered atoms induced by low energy heavy ion distribution *Rad. Effects & Defects in Solids* **160** 337-47

[29] Nikiporetz E, Semenov A, Shkarban I, Khartova E "Sputtering process of BN based ceramic by the flows of noncompensated charge plasma," *30th Int.Electric Propulsion Conf. (Florence, Italy)* IEPC-2007-7
[30] Garnier Y, Viel V, Roussel J-F and Bernard J 1999 Low-energy xenon ion sputtering of ceramics investigated for stationary plasma thrusters *J. Vac. Sci. Tech. A* **17** 3246-54
[31] Bachmann L and Shin JJ 1966 Measurement of the Sticking Coefficients of Silver and Gold in an Ultrahigh Vacuum *J. Appl. Phys* **37** 242-6.
[32] http://srdata.nist.gov/xps/
[33] Abgaryan V K, Mikheev S Yu, Prokofiev M V, Ryzhov Yu A and Shkrban I I 2006 Mass spectra of particles emitted from ceramic surfaces irradiated by plasma flows *Bulletin of the Russian Academy of Sciences: Physics (Izvestiya Rossiiskoi Akademii Nauk. Seriya Fizicheskaya)* **70** 879-82 (in Russian).
[34] Sigmund P 1969 Theory of sputtering I: sputtering yield of amorphous and polycrystalline targets *Phys. Rev.* **184** 383-416
[35] Wehner G K and Rosenberg D 1960 Angular distribution of sputtered material *J. App. Phys.* **31** 177-9
[36] Chini T K Tanemura M and Okuyama F 1996 Angular distribution of sputtered Ge atoms by low keV Ar+ and Ne+ ion bombardment *Nucl. Instr. and Meth. in Phys. Res. B* **119** 387-91
[37] Yamamura Y and Muraoka K 1989 Over-cosine angular distributions of sputtered atoms at normal incidence *Nucl. Instr. and Meth. in Phys. Res. B* **42** 175-81
[38] Yamamura Y 1981 Contribution of anisotropic velocity distribution of recoil atoms to sputtering yields and angular distributions of sputtered atoms *Rad. Eff.* **55** 49–55
[39] Yamamura Y 1982 Theory of sputtering and comparison to experimental data *Nucl. Instr. and Meth.* **194** 515–22
[40] Zhang Z L and Zhang L 2004 Anisotropic angular distributions of sputtered atoms *Rad. Eff. and Def. in Solids* **159** 301-7
[41] Zhang J, Bhattachargee S, Shutthanandan V and Ray P K 1997 Sputtering investigation of boron nitride with secondary ion and secondary neutral mass spectrometry *J. Vac. Sci. Tech. A* **15** 243-7
[42] Yamamura Y and Tawara H 1996 Energy Dependence of Ion-Induced Sputtering Yields from Monatomic Solids at Normal Incidence *At. Data Nucl. Data Tables* **62** 149-253.
[43] Yamamura Y, Itikawa Y and Itoh N 1983 Angular Dependence of Sputtering Yields of Monatomic Solids *Institute for Plasma Physics Report* IPPJ AM-26,.
[44] Doerner R P, Whyte D G and Goebel D M 2003 Sputtering Yield Measurements During Low Energy Xenon Plasma Bombardment *J. Appl. Phys.* **93** 5816-23.
[45] Bohdansky J A1984 Universal Relation for the Sputtering Yield of Monatomic Solids at Normal Ion Incidence *Nucl. Instr. and Meth. in Phys. Res. B* **2** 587–91.
[46] Semenov A and Shkarban I 1991 Ion Beam Sputtering of the Surfaces of Ion and Plasma Sources *Rocket and Space Engineering: Rocket Engines and Power Plants,* No.3, 42-53 (in Russian).
[47] Abashkin V, Gorshkov O, Lovtsov A and Shagaida A 2007 Analysis of Ceramic Erosion Characteristic in Hall-Effect Thruster with Higher Specific Impulse *30th Int. Electric Propulsion Conf. (Florence, Italy)* IEPC-2007-133
[48] Kim V, Kozlov V, Semenov A and Shkarban I 2001 Investigation of the Boron Nitride Based Ceramics Sputtering Yield Under it's Bombardment by Xe and Kr Ions *27th Int. Electric Propulsion Conf. (Pasadena, CA)* IEPC-2001-073.